

Electronic Supplementary Information (ESI) for

Stop-and-go, stepwise and “ligand-free” nucleation, nanocrystal growth and formation of Au-NPs in ionic liquids (ILs)

Engelbert Redel¹, Michael Walter^{2*}, Ralf Thomann², Laith Hussein², Michael Krüger² and Christoph Janiak^{1*}

¹Institut für Anorganische und Analytische Chemie, Universität Freiburg, Albertstr. 21, D-79104 Freiburg, Germany.

Engelbert Redel: Tel: int+416 7683586; E-mail: engelbert_redel@web.de

Christoph Janiak: Tel: int+49 761 2036127; E-mail: janiak@uni-freiburg.de

²FMF (Freiburger Material Forschungszentrum), Stefan-Meier-Str. 21, and IMTEK (Institut für Mikrosystemtechnik), Georg-Köhler Alle 103, Universität Freiburg, D-79104 Freiburg, Germany,

Michael Walter Tel: int+49 761 2034758; E-mail: michael.walter@mf.uni-freiburg.de

Ralf Thomann: Tel: int+49 761 2035379; E-mail: ralf.thomann@mf.uni-freiburg.de

Laith Hussein: Tel: int+49 761 2034759; E-mail: laith.hussein@mf.uni-freiburg.de

Michael Krüger: Tel: int+49 761 2034755; E-mail: michael.krueger@mf.uni-freiburg.de

Content

Experimental details	1
Pictures of color change (Fig. 1)	2
Additional pictures from TEM & HRTEM (Fig. S2-S9)	3
TED analysis by diffraction rings (Table S1)	10
Additional UV/VIS spectra (Fig. S10-S13)	11
Computational method and DFT calculations (Table S2 and S3)	16

Experimental details

Materials and instrumentation: KAuCl₄ (99 % p.a.) and ZnCl₂ (anhydrous) were obtained from Aldrich and Strem, *n*-butyl-imidazole (p.a.) was obtained from Aldrich, the ionic liquids (ILs) *n*-butyl-methyl-imidazolium tetrafluoroborate (BMIm⁺BF₄⁻), *n*-butyl-methyl-imidazolium hexafluorophosphate (BMIm⁺PF₆⁻) and trifluoromethanesulfonate (BMIM⁺OTf⁻) from IoLiTec (H₂O content << 100 ppm; Cl⁻ content << 50 ppm). All manipulations were done using Schlenk techniques under argon. The ionic liquids were dried at high vacuum (10⁻³ mbar) for several days to avoid especially in the case of BMIm⁺BF₄⁻ the hydrolysis to HF.

Synthesis details:

Au-NPs were obtained by the reduction of KAuCl₄ with SnCl₂ in different ILs BMIm⁺BF₄⁻, BMIm⁺PF₆⁻ or BMIm⁺OTf⁻. The salts were dissolved separately under argon atmosphere in the dried and deoxygenated ionic liquid. KAuCl₄ (30.0 mg, 0.08 mmol, dissolved in 3.0 g IL) was added dropwise to a SnCl₂/IL solution (20.0 mg, 0.1055 mmol, dissolved in 2.0 g IL) at room temperature under argon atmosphere and at a constant stirring rate (1000 rpm). Molar Au:Sn ratios of 1:24, 1:12, 1:10, 1:8, 1:6, 1:5, 1:4.5, 1:4 and 1:3, corresponding to defined volumes of KAuCl₄/IL between 0.15 – 1.5 mL (see TEM pictures in this Supporting Information Fig. S2 - Fig. S8) were chosen in BMIm⁺BF₄⁻ (δ = 1.208 g/cm³).

When BMIm⁺Cl⁻ (>35 mg, 0.20 mmol) was added in a molar ratio of more than 1:22 to BMIm⁺BF₄⁻ (1.0 g, 4.42 mmol) no gold particles larger than 1 nm could be observed (see this Supporting Information Fig. S9).

Post synthetic treatment/stabilization with *n*-butyl-imidazole

The synthesized Au-NPs in ILs are only *kinetically* stabilized, hence, *n*-butyl-imidazole (BIm) was used to stop a continued aggregation (secondary growth) for the subsequent optical measurements. The similarity of BIm with the IL-cation BMIm⁺ aids in the miscibility/solubility and minimal IL network disturbance to function as a capping ligand to the Au_n surface. Furthermore, dilution with *n*-butyl-imidazole was advantageous for the UV/VIS measurements because of its identical absorbance properties to BMIm⁺X⁻ (X⁻ = BF₄, PF₆, OTf).

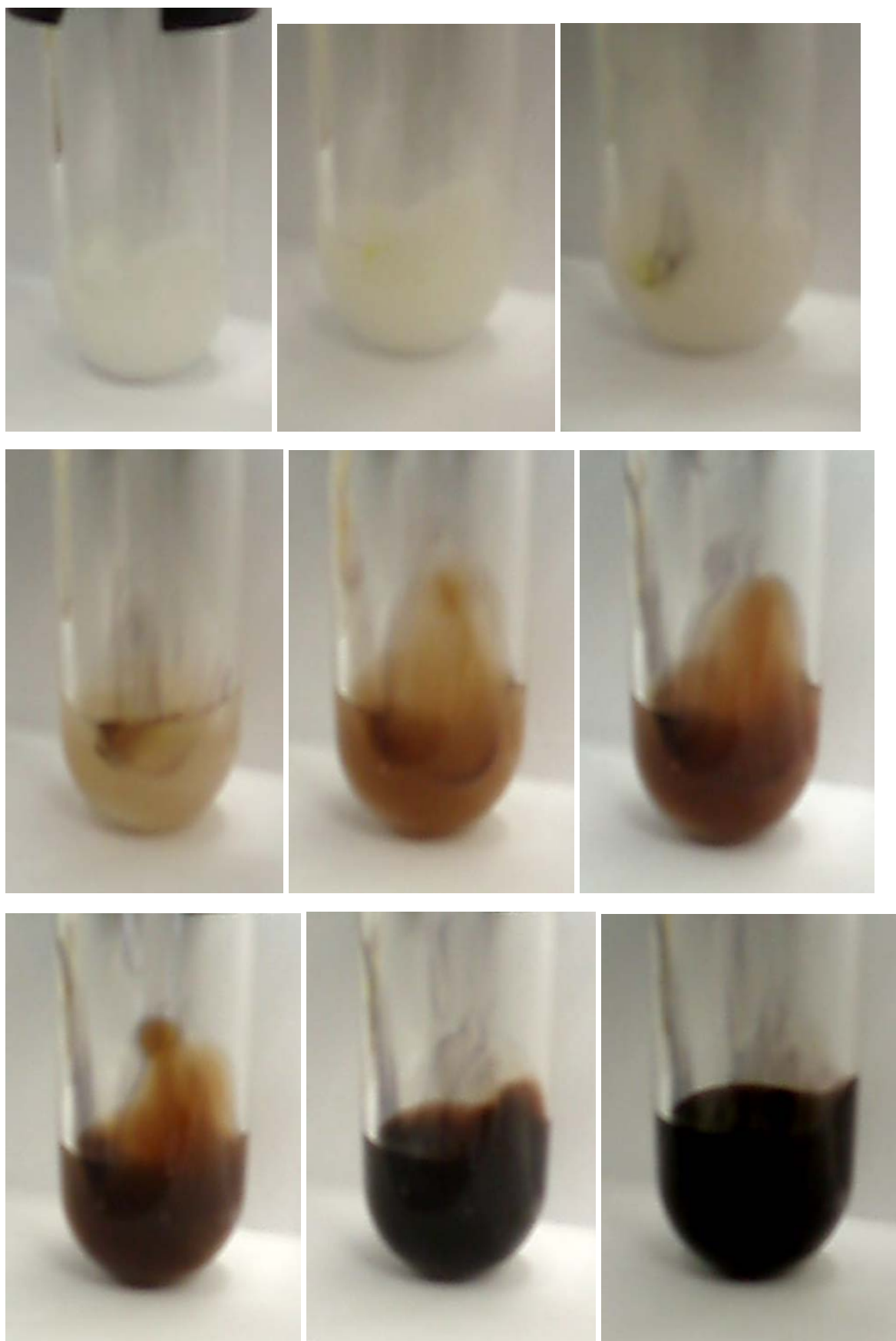


Figure S1. Au growth process and color change (overview).

Additional pictures from TEM & HRTEM and UV/VIS spectra

Transmission electron microscopy (TEM and TED) and high resolution transmission electron microscopy (HRTEM) photographs were taken at room temperature from a carbon-coated copper grid by a Zeiss LEO 912 (TEM) transmission electron microscope operating at an accelerating voltage of 120 kV and on a HRTEM Phillips CEM 200 ST high resolution transmission electron microscope operating at an accelerating voltage of 200 kV.

Figure S2-S8 are HR/TEM and TED measurements belonging to Table 1.

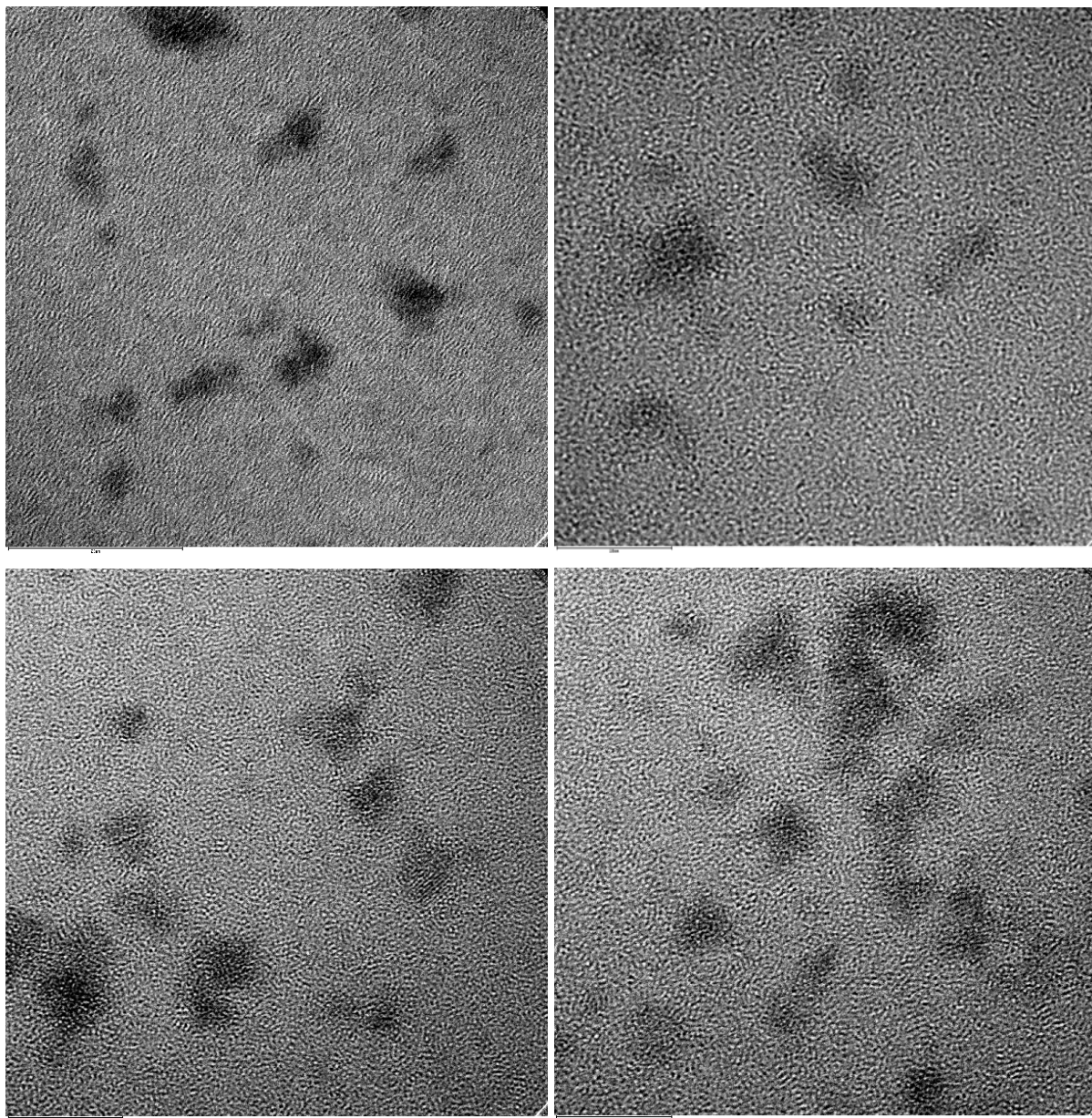


Figure S2. HRTEM photographs of Au nanoparticles / Au:Sn (1:24) in $\text{BMIm}^+\text{BF}_4^-$, see the scale bar of 10 nm below the bottom left corner of each photograph. (Table 1, entry 1).

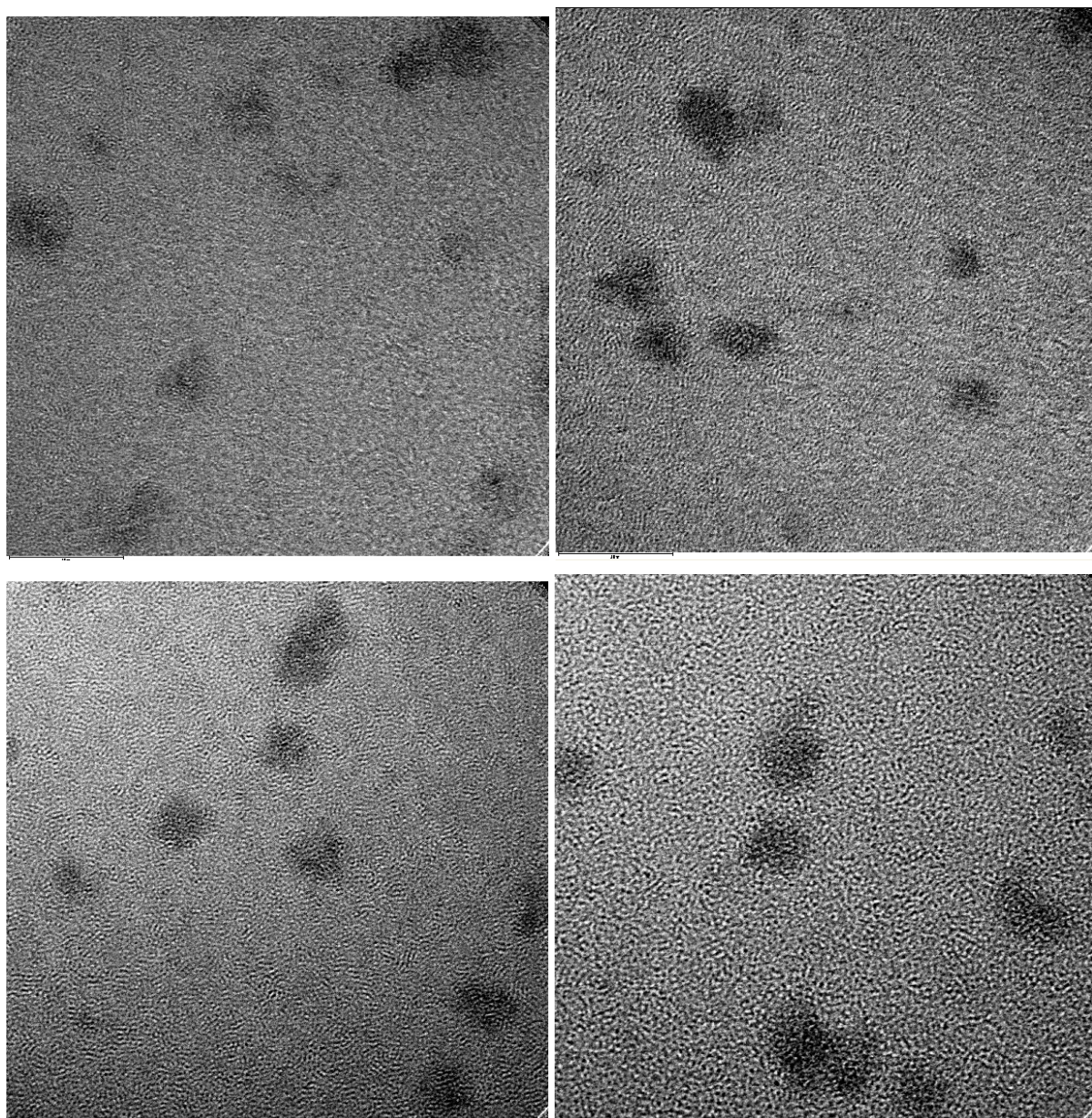
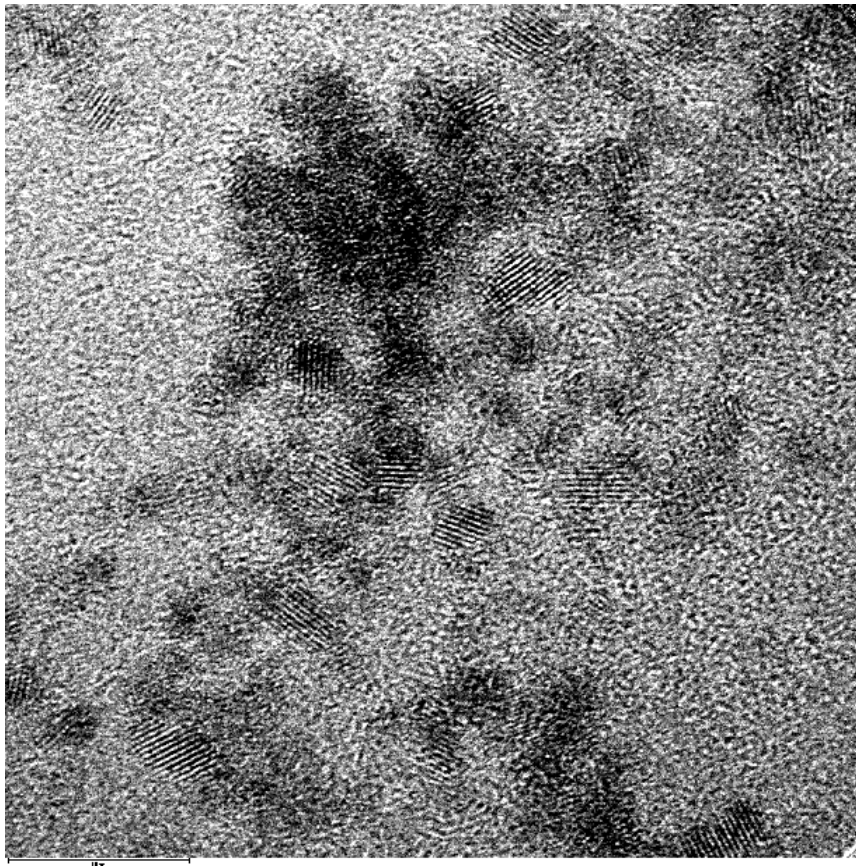
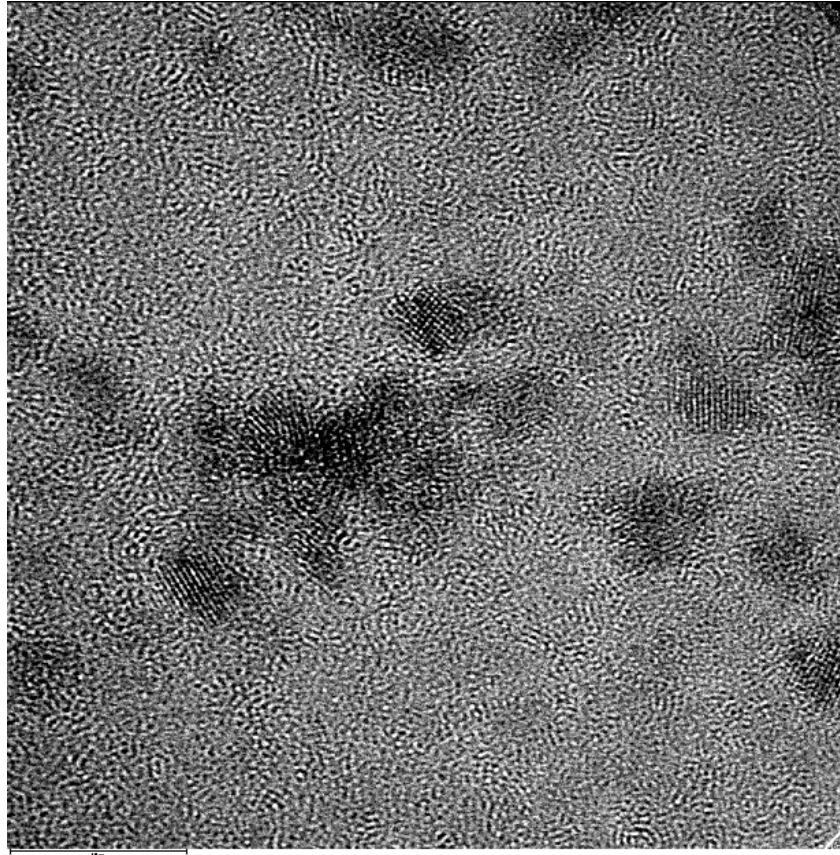


Figure S3. HRTEM photographs of Au nanoparticles / Au:Sn (1:12) in $\text{BMIm}^+\text{BF}_4^-$, see the scale bar of 10 nm below the bottom left corner of each photograph. (Table 1, entry 2).



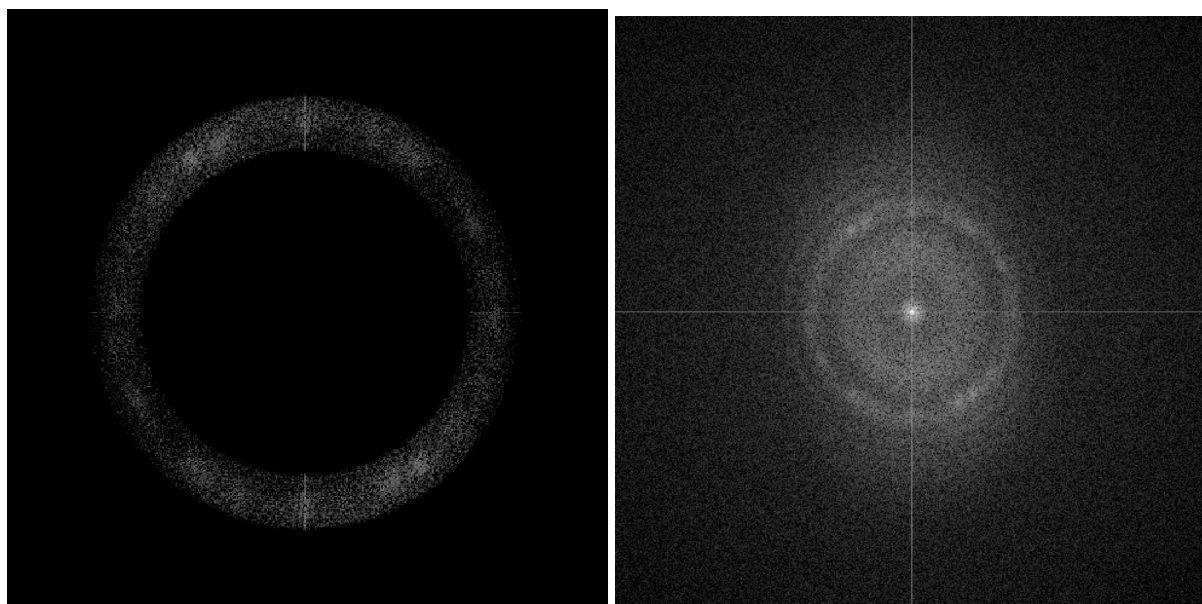
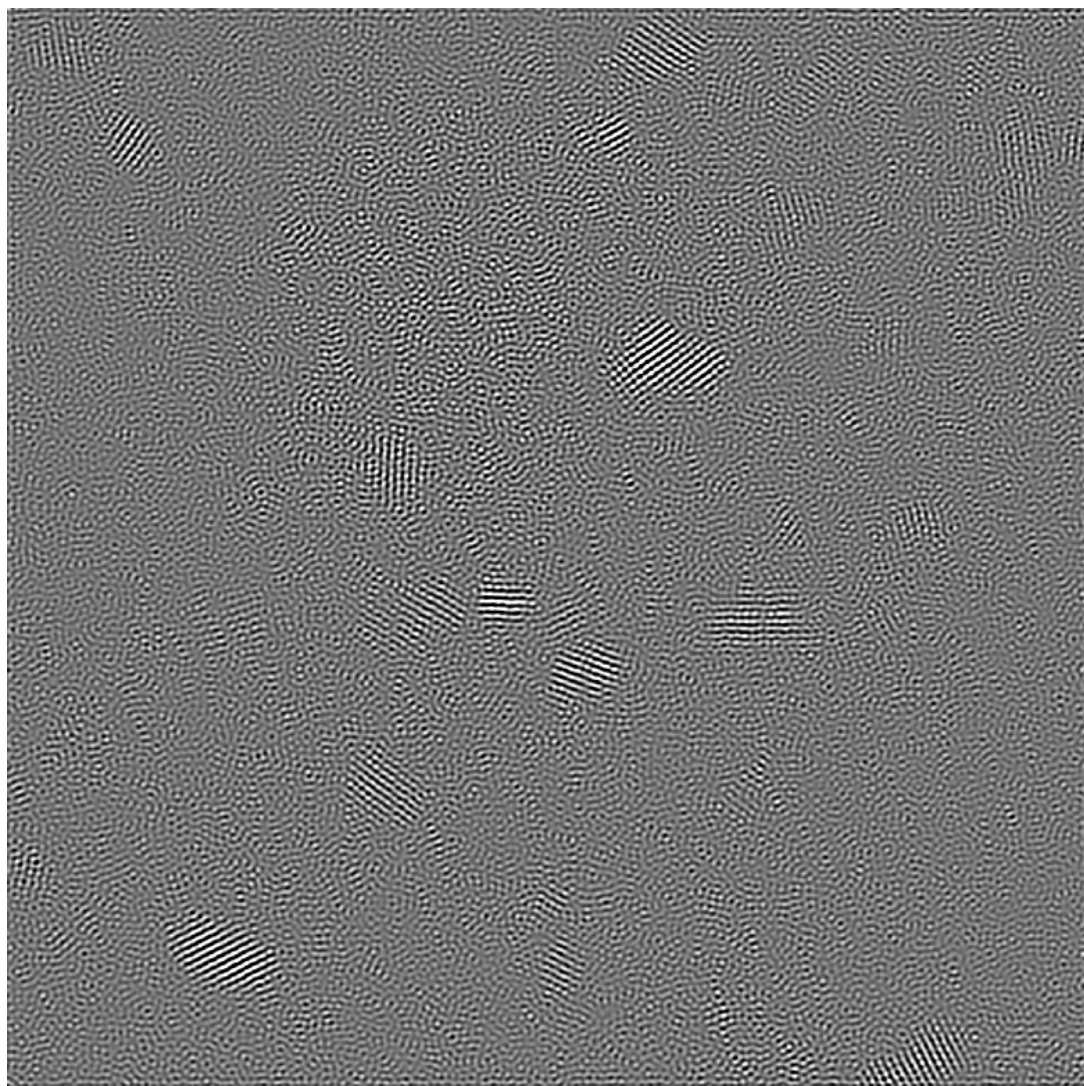


Figure S4. HRTEM & FFT filtered photographs of Au-NPs / Au:Sn (1:6) in $\text{BMIm}^+\text{BF}_4^-$, see the scale bar of 10 nm below the bottom left corner of each photograph. (Table 1, entry 3).

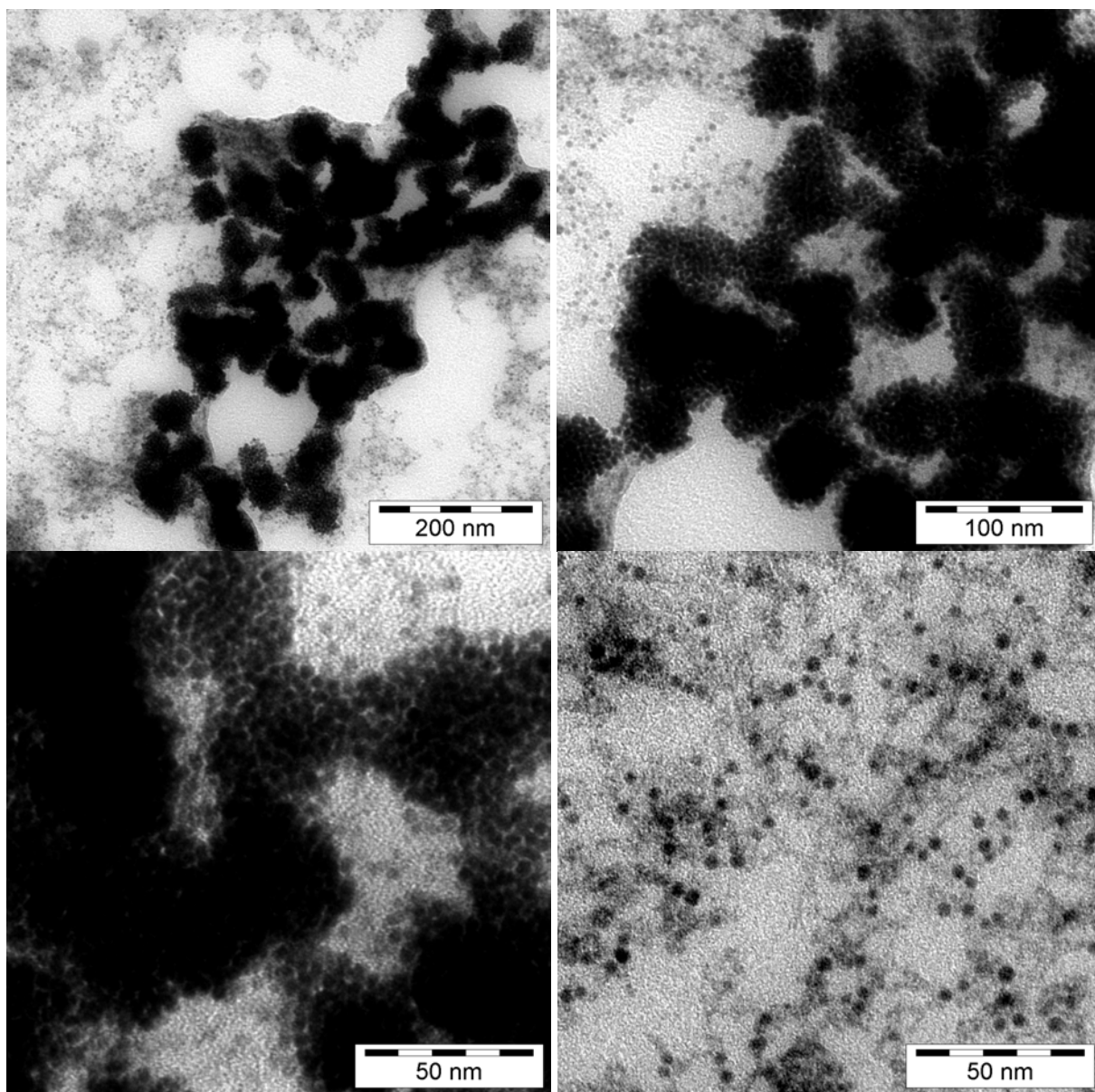


Figure S5. TEM photographs of Au nanoparticles / Au:Sn (1:5) in $\text{BMIm}^+\text{BF}_4^-$ (Table 1, entry 4).

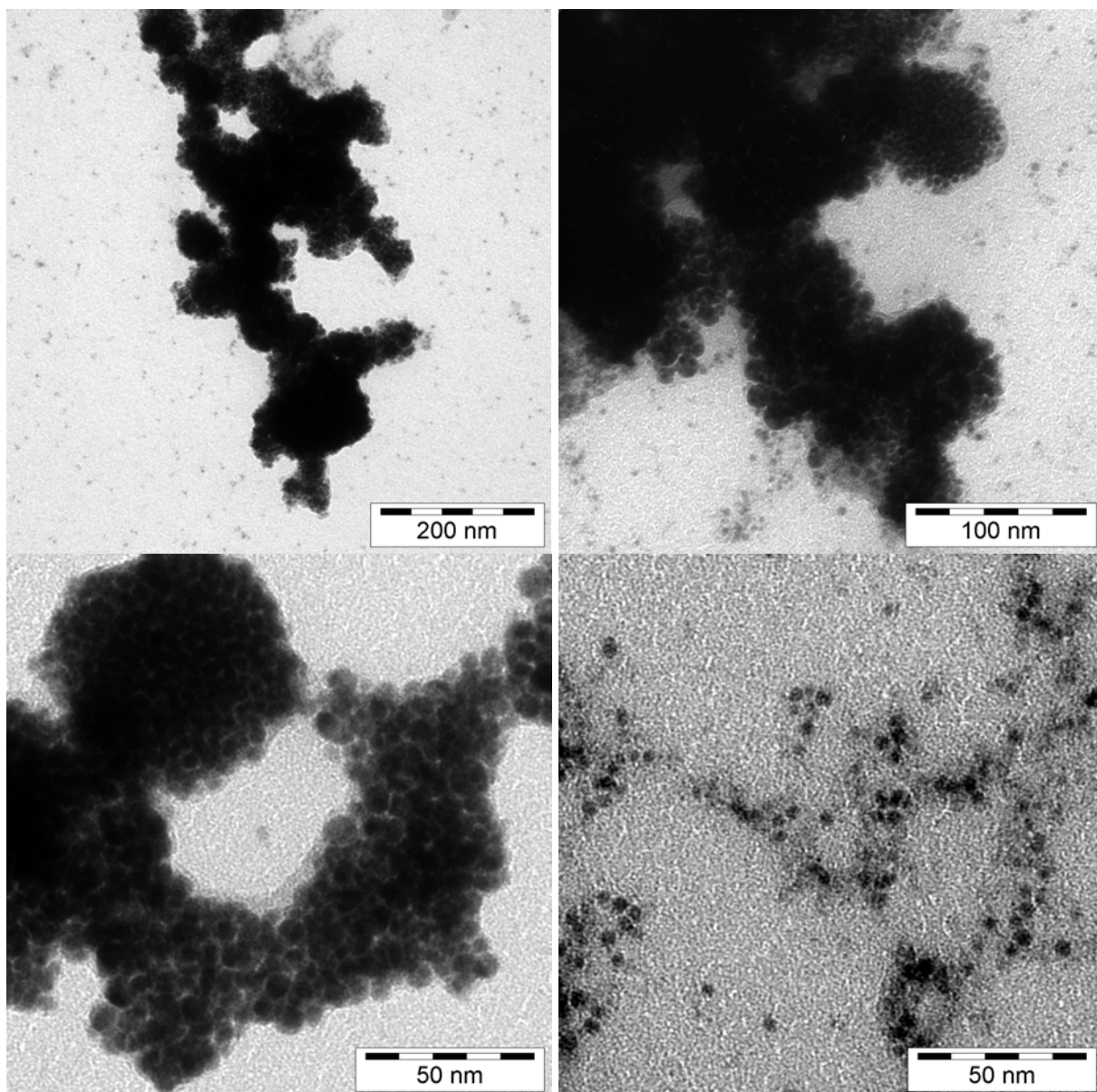


Figure S6. TEM photographs of Au nanoparticles / Au:Sn (1:4.5) in BMIm⁺BF₄⁻ (Table 1, entry 5)

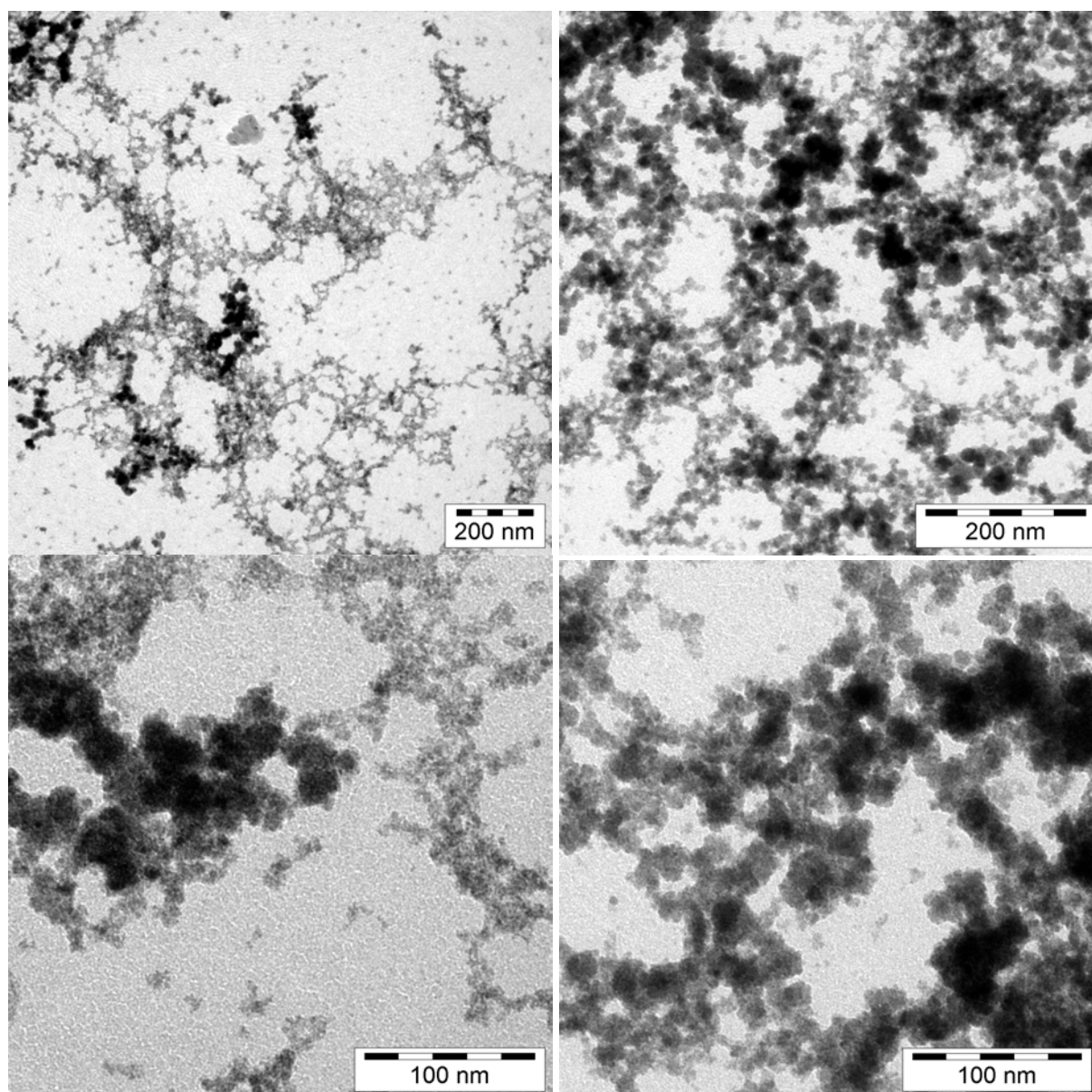


Figure S7. TEM photographs of Au nanoparticles / Au:Sn (1:4) in $\text{BMIm}^+\text{BF}_4^-$ (Table 1 entry 6).

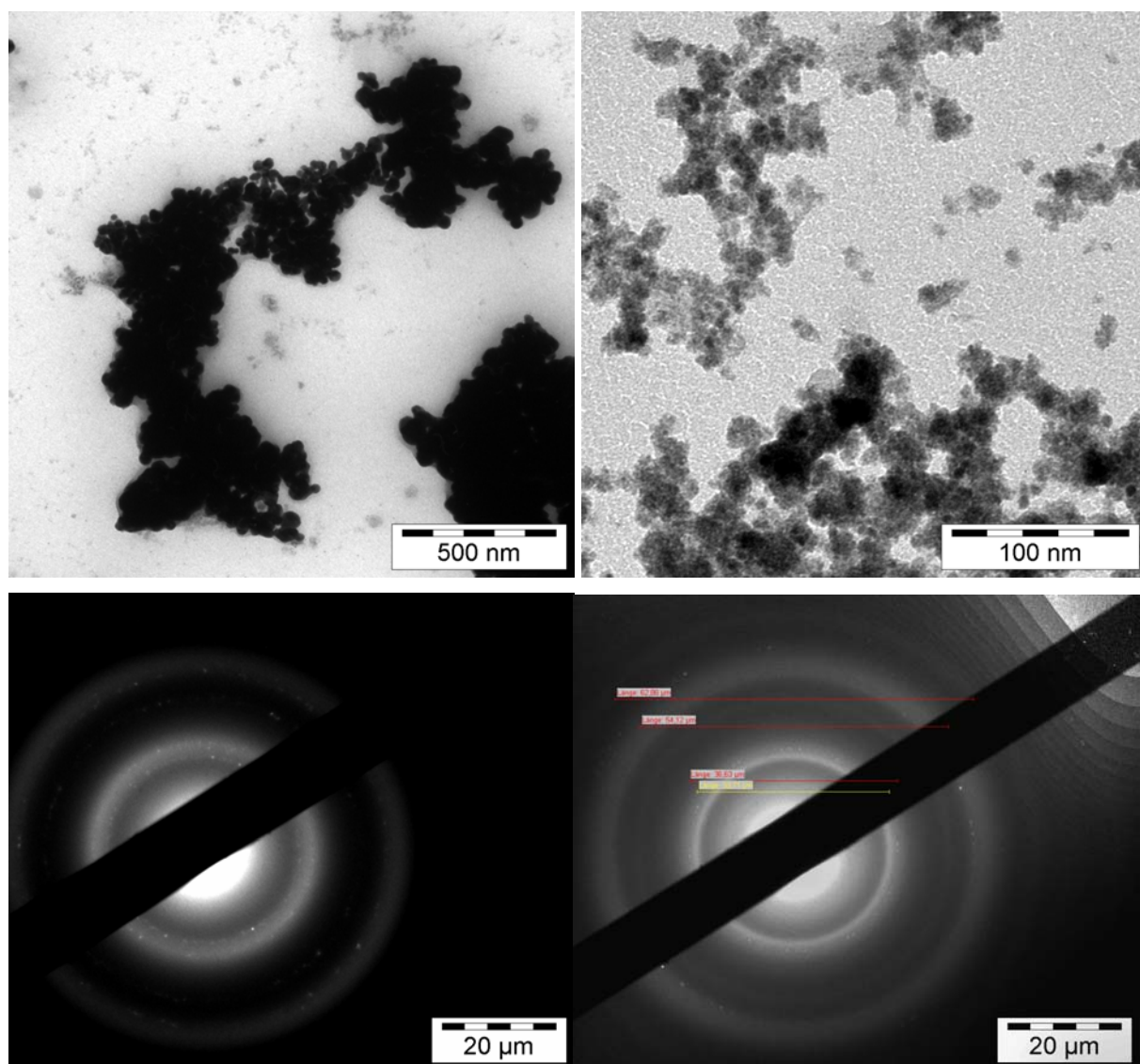


Figure S8. TEM photographs of Au nanoparticles / Au:Sn (1:3) in $\text{BMIm}^+\text{BF}_4^-$ (Table 1, entry 7). TED shows crystalline particles whose parameters correspond to the gold metal lattice, see **Table S1**.

Table S1. Diffraction data for Au from TED Figure S8

Intensity	D (Å) from TED	D(Å) STOIE Database	hkl
100 %	2.3374	2.3550	(111)
52 %	2.1514	2.0390	(200)
32 %	1.4561	1.4420	(220)
36 %	1.2536	1.2300	(311)

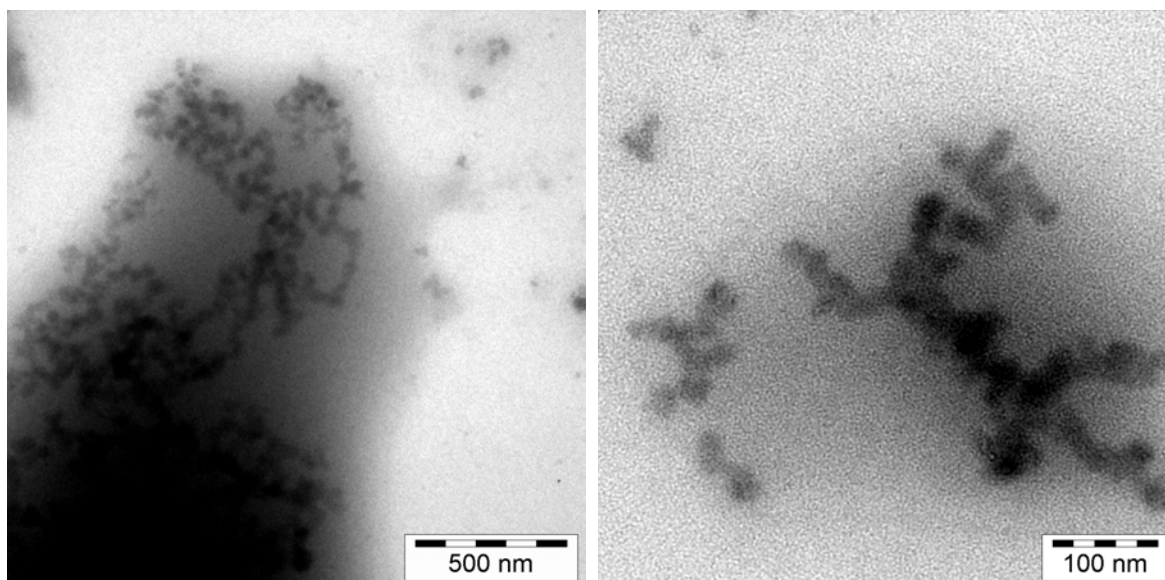


Figure S9. TEM photographs of Au nanoclusters in $\text{BMIm}^+\text{BF}_4^-$ in the presence of BMIm^+Cl^- . TEM pictures with particles of median diameter of less than 1.5 nm show electron dense cloudy structures due to scattering by the surrounding IL so that resolution of the TEM is limited and particles below 1.5 nm are hardly resolved.

Additional pictures and UV/VIS measurements

UV/VIS absorption measurement on Au-NP dispersions were done with a J&M *TIDAS* UV/VIS spectrometer in the wavelength range between 300 and 800 nm.

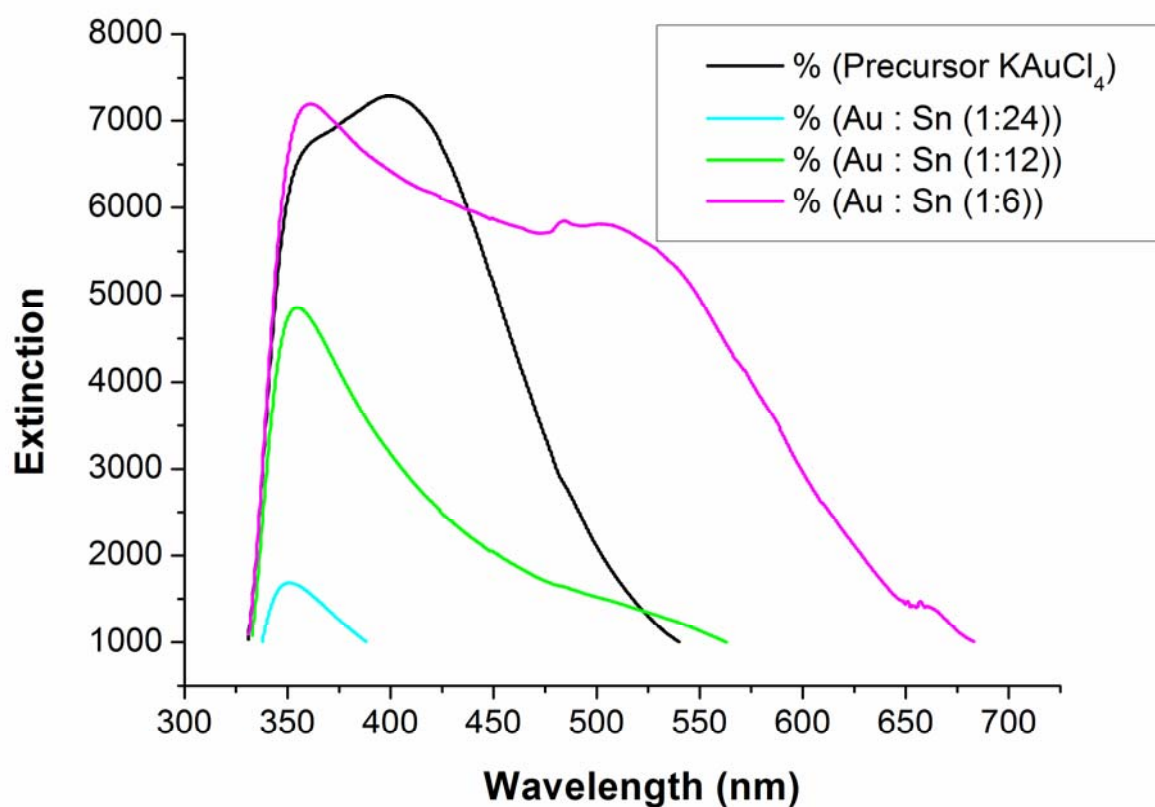
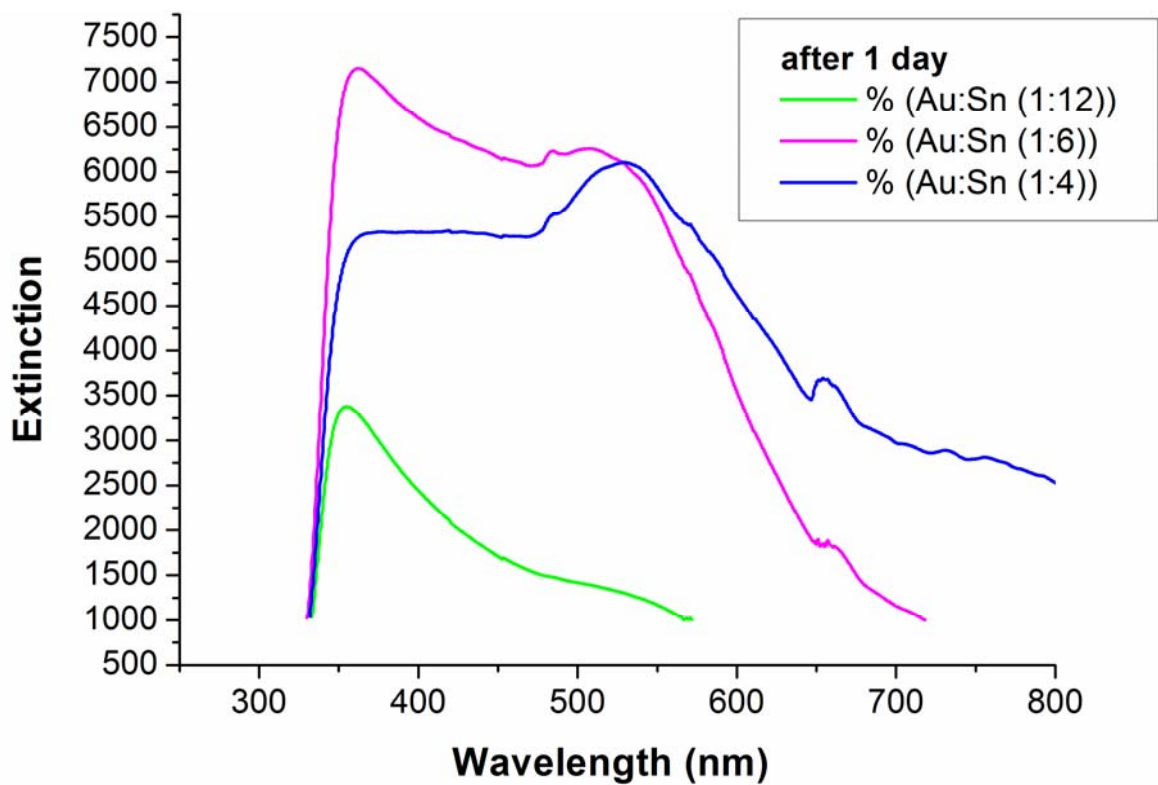
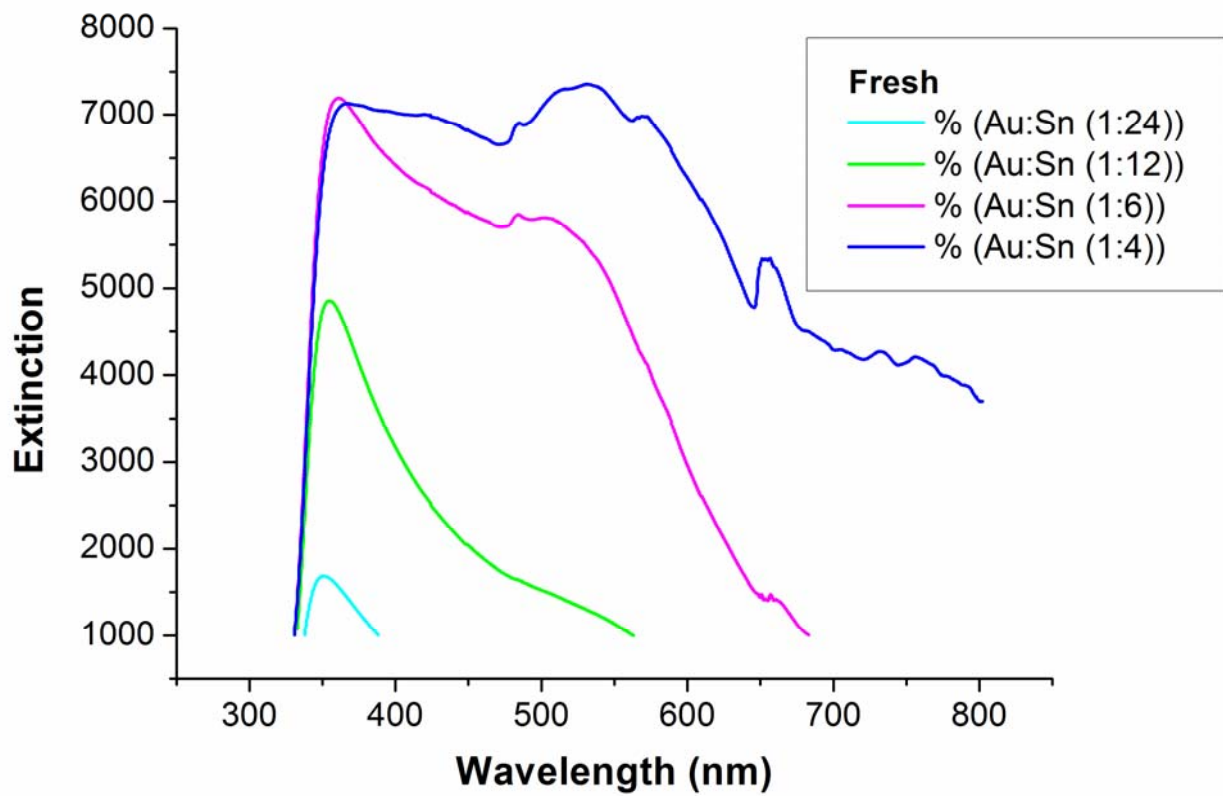


Figure S10. UV/VIS spectra of Au-precursor (KAuCl_4) and Au-NPs after reduction.



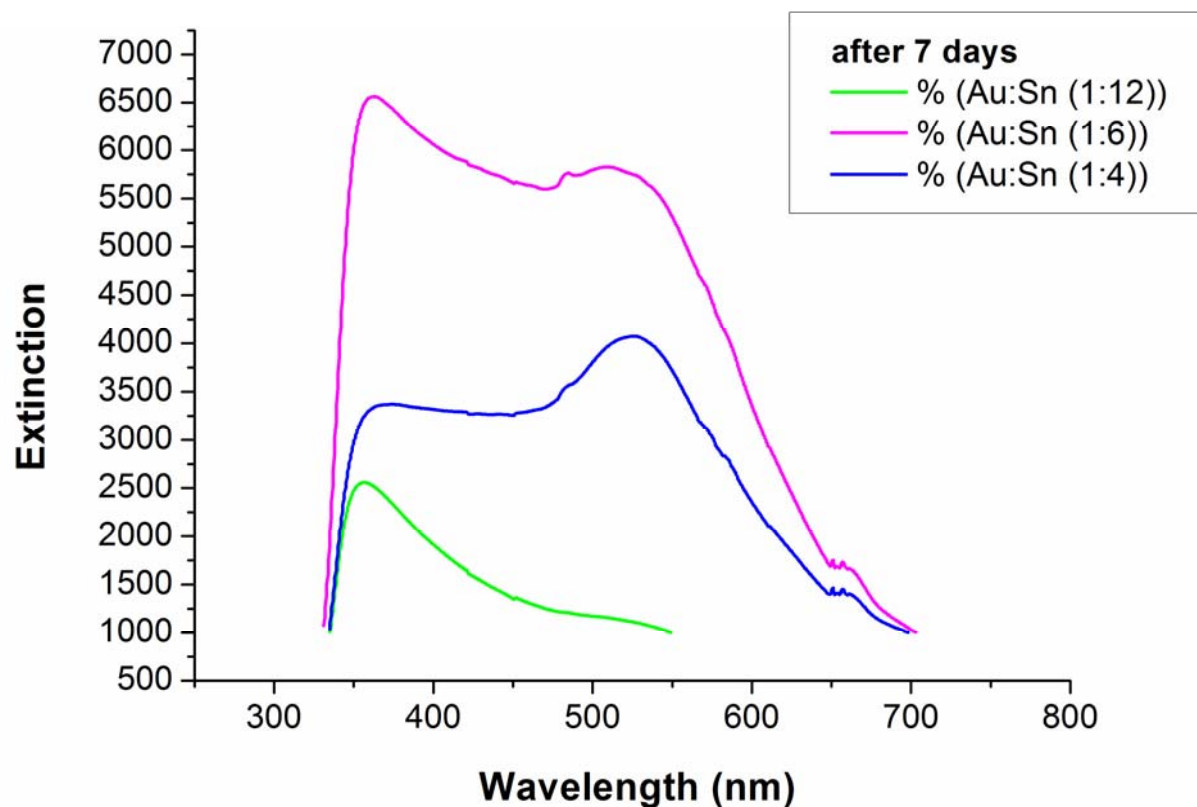
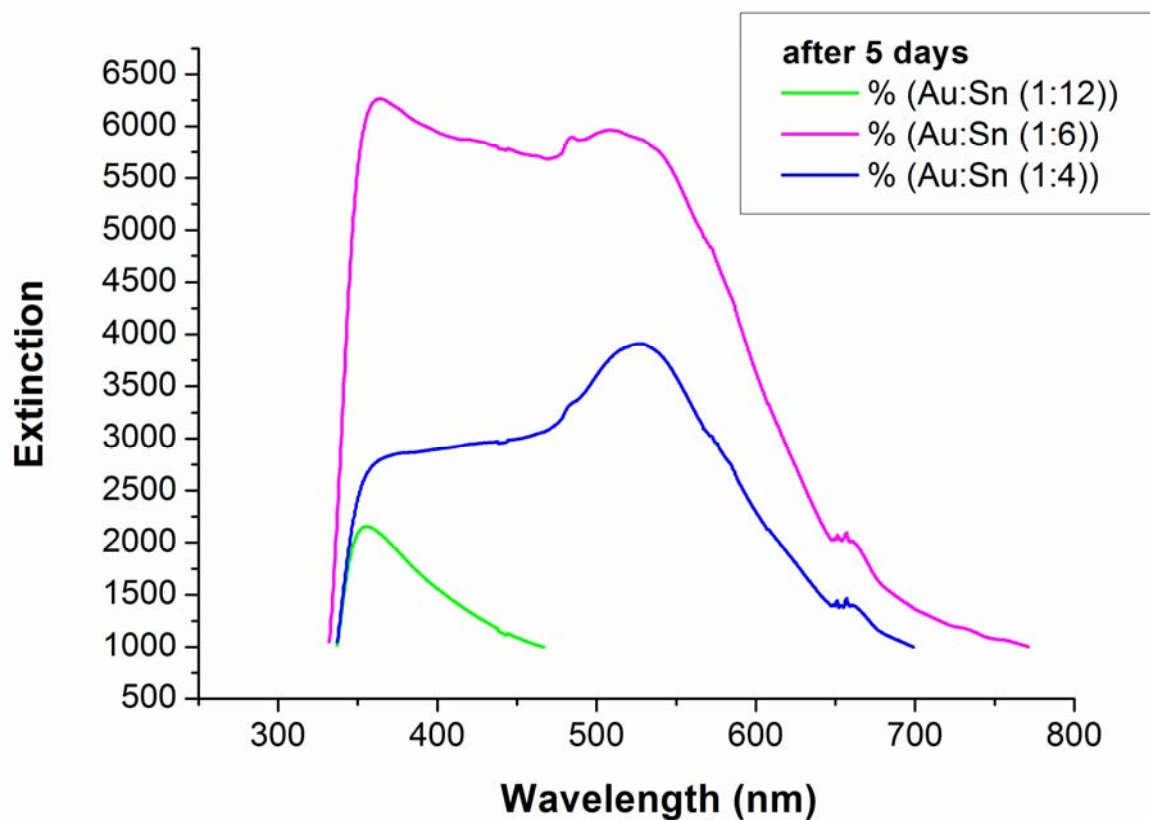
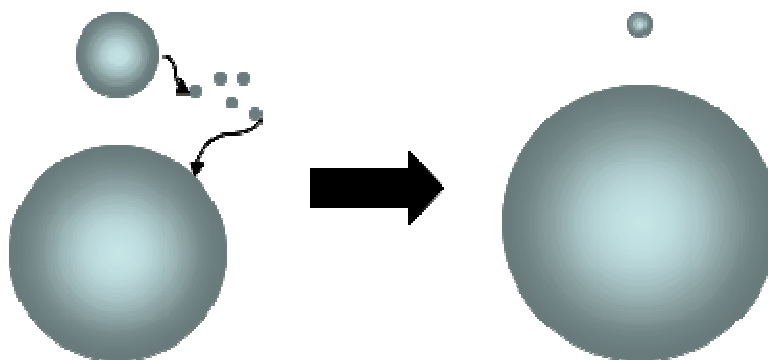


Figure S11. UV/VIS spectra of Au metal nanoparticles from $\text{BMIm}^+\text{BF}_4^-$, stabilized and dispersed in *n*-butyl-imidazole; fresh and after 1, 5 and 7 days.

In Figure S11, the absorption peak at 520 nm is the strongest one for a fresh sample at the molar ratio of Au to Sn about 1:4, but increases in intensity with time when the molar ratio of Au:Sn is about 1:6.

This is based on the principals of the Ostwald ripening: Ostwald ripening is a thermodynamically-driven spontaneous process and occurs because larger Au particles are more energetically favored than smaller Au particles. This stems from the fact that molecules on the surface of a particle are energetically less stable than the ones already well ordered and packed in the interior. Large Au particles, with their lower surface to volume ratio, results in a lower energy state (and have a lower surface energy). As the system tries to lower its overall energy, molecules on the surface of a small (energetically unfavorable) particle will tend to detach and diffuse through solution and then attach to the surface of larger particle. Therefore, the number of smaller particles continues to shrink, while larger particles continue to grow (see Scheme S1 below).

We were able to observe fast Ostwald ripening for the large Au-NPs samples, e.g. Au:Sn = 1:4, ~22 nm. This thermodynamically driven process becomes faster as the Au particle size increases. For the smaller particles (Au:Sn = 1:6, ~5 nm and 1:12 ~1-3 nm) Ostwald ripening is very slow for the ~5 nm particles (or even could not be observed for the ~1-3 nm particles). This can be described by a thermodynamic equilibrium for samples with small and ultra-small particles, as a result that the difference in surface energy between small (~5 nm) and ultra-small (~1-3 nm) is low, in contrast to the difference between ultra-small (~1-3), middle-sized (ca. ~10 nm) and large Au particles (>20 nm).



Scheme S1: Schematic presentation of the Ostwald ripening. Source: <http://en.wikipedia.org/wiki/File:Ostwaldpic.png>

If surface and secondary growth are of comparative rate a bimodal particle size distribution will be obtained (Table 1). Normally the secondary growth process is faster than surface growth and is slowed down until it is finally stopped by the presence of a surface-capping ligand. Here, ILs are not acting as strong capping ligands (Fig. 4), but as a *kinetically* stabilizing, dynamic molecular network in which the reduced Au⁰ atoms and clusters can move by diffusion and cluster together. The stabilizing effect is enabled through the high ionic charge, high polarity, high dielectric constant and formation of supramolecular network structures by the ILs. Thus, the Au nanocrystals can nucleate and grow in a step-by-step manner through the controlled addition of new gold precursor material in an efficient way. At the desired size the Au-NPs can be *thermodynamically* stabilized through the post-synthetic addition of a capping ligand, e.g. *n*-butylimidazole, see ESI. The Au_n surface can be covered and, thus, secondary growth process can be inhibited by adding free Cl⁻ to the reaction medium (see ESI Fig. S9). Due to the high affinity of Cl⁻ anions to the surface of the gold seeds, a further surface growth or agglomeration process does not occur. In comparison to other stabilizing substrates like phosphane, citrate or IL-anions, only Cl⁻ can inhibit Au-growth in its nucleation stages (Fig. 4).

In conclusion we describe here a simple and reproducible method for a "ligand-free", stop-and-go step-by-step nucleation and nanocrystal growth process of Au nanoparticles in ionic liquids as a

"novel nanosynthetic template" through a controlled addition of the reactants. This Au-NP growth process can be stopped and resumed at any different intermediate color step and nanoparticle-size, which enables an investigation of the Au-NP nuclei and nanocrystal formation (from amorphous to crystalline). A DFT-calculated weak binding energy (BE) of the IL-BF₄ anion to gold clusters never exceeds the gold-gold interaction and supports the model of a dynamic Au_n⋯IL stabilization and a dynamic nucleation and nanocrystal growth process.

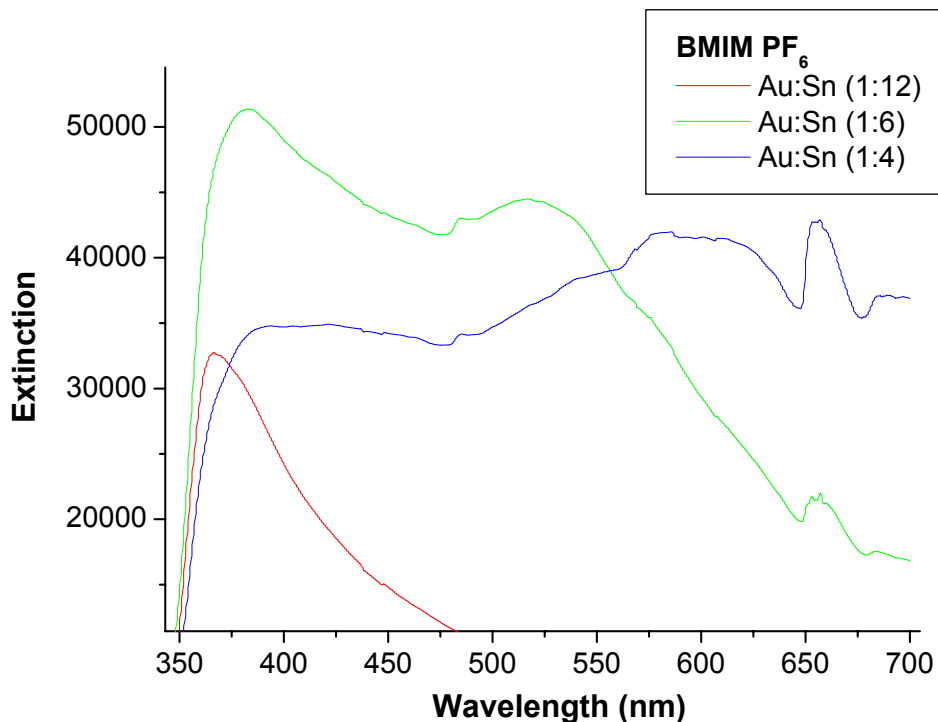


Figure S12. UV/VIS spectra of Au metal nanoparticles in BMIm⁺PF₆⁻.

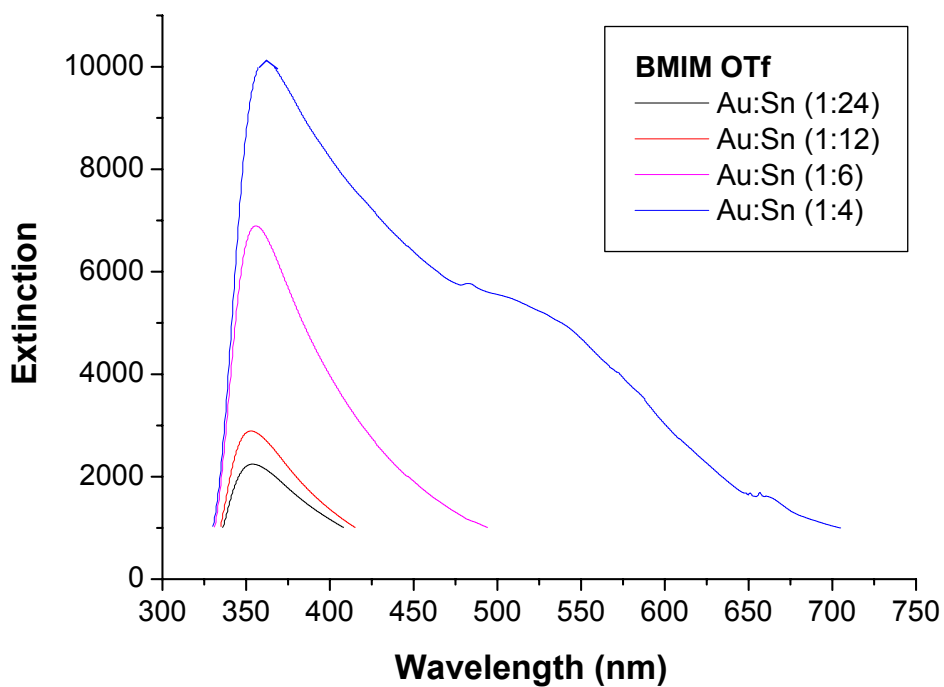


Figure S13. UV/VIS spectra of Au metal nanoparticles in BMIm⁺OTf⁻.

Computational method and DFT calculations:
Binding of small Gold clusters to various stabilizing units

The BE is defined as the difference of the relaxed energies of the gas phase anions and the Au_n clusters to the energy of their adduct. The gold clusters considered here are clusters which are known to be formed in the gas phase in their neutral state. The cluster sizes Au_n , $n = 1, 2, 3, 6, 19$ were chosen because the ground state structures in the gas phase of both Au_n and Au_{n+1} are known in the literature.¹

Therefore the binding energy of the stabilizing substrates can be directly compared to the addition energy of a single Au^0 atom onto the cluster. The selection also contains both closed and open electronic shell clusters, serving as models for molecular and metallic clusters, respectively.

The Kohn-Sham DFT calculations were performed with the program package GPAW.² The projector augmented wave method³ was used and the smooth wave functions were represented on uniform real space grids. This approach provides a single convergence parameter, the grid-spacing, to control the accuracy of discretization. The calculations were carefully tested on numerical convergence and found to be converged at a grid-spacing of 0.18 Å. The exchange-correlation energy was approximated in a generalized gradient approximation (GGA) as proposed by Perdew, Burke and Ernzerhof (PBE).⁴ The results were cross-checked using the GGA proposed by Perdew and Wang^[5] and the meta-GGA functional as proposed by Tao, Perdew, Staroverov and Scuseria.⁶ No qualitative difference in the BE behavior by changing the functional was observed (see Table S2 and Table S3). Structures containing an even number of gold atoms were treated as spin-unpolarized, whereas structures containing an odd number of gold atoms were treated in a spin-polarized calculation. The adducts of clusters connected to the ions or free bases were geometry optimized without any symmetry restriction. The structures were considered to be relaxed if the forces fell below 0.05 eV/Å.

The Tables S2 and S3 show the binding energies of various stabilizing neutral and anionic molecules for different cluster sizes. All energies are evaluated at PBE relaxed geometries and using the PBE molecular orbitals.

Table S2. Binding Energy for Au and Au_2 (see Figure 4). All values in eV (1 eV = 23.06 kcal/mol).

	Au			Au_2		
	PBE	PW91 ^a	TPSS ^a	PBE	PW91 ^a	TPSS ^a
Au_n to Au_{n+1}	2.28	2.31	2.24	1.25		
Cl^-	1.49	1.51	1.36	2.49	2.52	2.41
citrate ⁻	0.88	0.91	0.83	1.85	1.88	1.76
PH_3	0.95	0.97	0.81	1.7	1.73	1.59
CO	0.7	0.72	0.53	1.67	1.69	1.45
NH_3	0.62	0.65	0.55	1.31	1.34	1.25
TOf^-	0.46	0.49	0.39	1.27	1.29	1.17
BF_4^-	0.34	0.35	0.3	1.02	1.04	1.02
PF_6^-	0.21	0.23	0.16	0.78	0.8	0.76
H_2O	0.2	0.22	0.22	0.68	0.7	0.66
$BMI m^+$	0.42	0.44	0.26	0.23	0.25	0.2

Table S3. Binding Energy for Au₆ and Au₁₉ (see Figure 4). All values in eV (1 eV = 23.06 kcal/mol).

	Au ₆			Au ₁₉		
	PBE	PW91 ^a	TPSS ^a	PBE	PW91 ^a	TPSS ^a
Au _n to Au _{n+1}	1.6	1.62	1.44	3.16	3.19	3.24
Cl ⁻	2.57	2.6	2.55	2.99	3.02	2.89
citrate ⁻	1.28	1.32	1.21	1.66	1.48	1.48
PH ₃	1.14	1.16	1	0.96	0.99	0.73
CO	1	1.02	0.82	0.82	0.84	0.66
NH ₃	0.9	0.92	0.82	0.76	0.79	0.68
TOF ⁻	1.2	1.22	0.99	1.36	1.37	1.24
BF ₄ ⁻	1.08	1.1	1.04	1.2	1.22	1.22
PF ₆ ⁻	0.84	0.86	0.78	0.98	1	0.93
H ₂ O	0.39	0.41	0.34	0.3	0.31	0.23
BMI ⁺	0.35	0.37	0.19	0.43	0.46	0.36

^a nonselfconsistent calculation using PBE geometries and wave functions

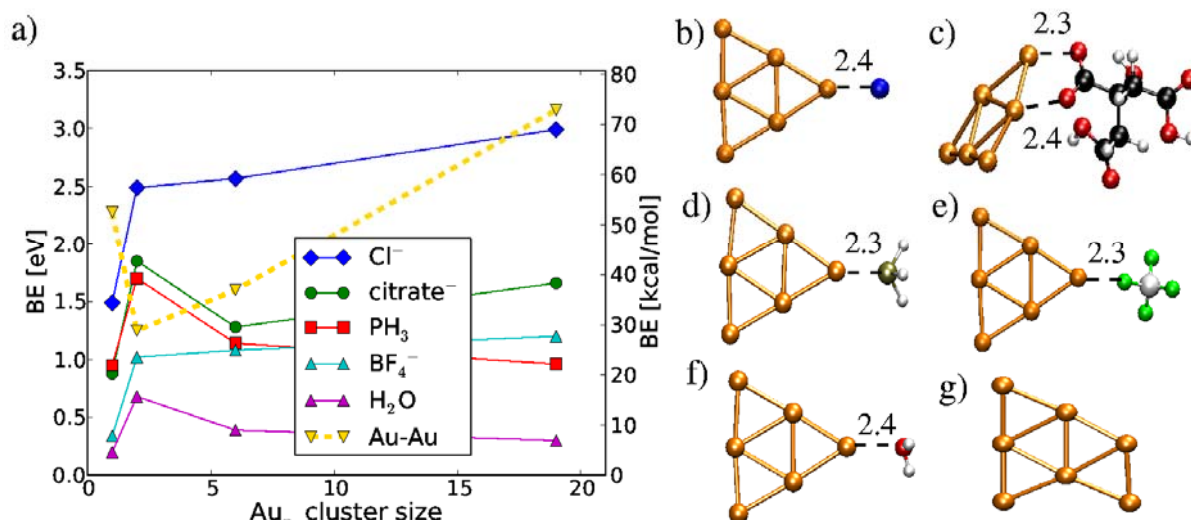


Fig. 4 (repeated from paper) **a**, Binding energies (BE) and addition energies depending on the cluster size. **b-f**, Relaxed configurations of Au₆ bound to **b**, Cl⁻, **c**, citrate⁻ (C₆H₇O₇⁻) **d**, PH₃, **e**, BF₄⁻ and **f**, H₂O. **g**, Relaxed configuration of Au₇. The bond lengths are given in Å.

- (1) C. W. Bauschlicher, S. R. Langhoff and H. Patridge, *J. Chem. Phys.*, 1990, **94**, 8378-8379; H. Häkkinen, U. Landmann, *Phys. Rev. B.*; 2000, **62**, R2287-R2290; P. Gruene, D. M. Rayner, B. Redlich, A. F. G. van der Meer, J. T. Lyon, G. Meijer and A. Fielicke, *Science*, 2008, **321**, 674-676.
- (2) Mortensen, J. J.; Hansen, L. B.; Jacobsen, K. W. *Phys. Rev. B.* **2005**, *71*, 035109, p.11.
- (3) Blöchl, P. E. *Phys. Rev. B.* **1994**, *50*, 17953-17979.
- (4) Perdew, J. P.; Burke, K.; Ernzerhof, M. *Phys. Rev. Lett.* **1996**, *77*, 3865-3868.
- (5) Perdew, J. P.; Wang, Y. *Phys. Rev. B.* **1992**, *45*, 13244-13249.
- (6) Tao, J.; Perdew, J. P.; Staroverov, V. N.; Scuseria, G. E. *Phys. Rev. Lett.* **2003**, *91*, 146401, p. 4.